

# Results and prospects of radiative and electroweak penguin decays at Belle II

Soumen Halder

(On behalf of the Belle II Collaboration)

Tata Institute of Fundamental Research, Mumbai 400005, India

The  $b \rightarrow s(d)$  quark-level transitions are flavor-changing neutral current processes, which are not allowed at tree level in the standard model. These processes are very rare and constitute a potential probe for new physics. Belle II at SuperKEKB is a substantial upgrade of the Belle experiment. It aims to collect  $50 \text{ ab}^{-1}$  of data by 2029 with a designed peak luminosity of  $8 \times 10^{35} \text{ cm}^{-2}\text{s}^{-1}$  that is 40 times more than its predecessor. It has been recording data since 2019 and during these early days of the experiment, efforts are being made to rediscover the aforementioned rare  $B$  decays. We report herein the rediscovery of  $B \rightarrow K^* \gamma$  and future prospects for radiative and electroweak decays at Belle II.

## I. INTRODUCTION

The flavor-changing neutral current processes mediated by  $b \rightarrow s(d)$  transitions are forbidden at tree level in the standard model (SM). These processes can however proceed via higher-order diagrams involving loops. Non-SM particles may contribute in such loops as shown in Fig. 1, which could suppress or enhance the amplitude of the decay rate. Hence, the decays mediated by  $b \rightarrow s(d)$  transitions have an excellent potential to probe new physics (NP). In this article, we report the current status and future prospect of Belle II for radiative penguin decays proceeding via  $b \rightarrow s(d)\gamma$  and for electroweak penguin decays mediated by  $b \rightarrow s(d)\ell^+\ell^-$  or  $b \rightarrow s(d)\nu\bar{\nu}$  transitions.

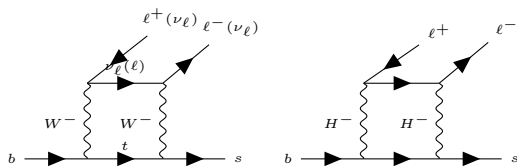


FIG. 1: Feynman diagrams of  $b \rightarrow s\ell^+\ell^-$  featuring a box diagram (left) and non-SM box diagram where  $W$  bosons are replaced by some non-SM particles such as charged Higgs bosons  $H^\pm$  (right).

## II. SUPERKEKB AND BELLE II

SuperKEKB is the next generation  $e^+e^-$  collider located at Tsukuba, Japan which has been upgraded to collide  $e^+$  and  $e^-$  beams at a rate 40 times higher than its predecessor KEKB. The Belle II detector placed at the collision point of SuperKEKB is a major upgrade of Belle. It has collected  $0.5 \text{ fb}^{-1}$  data during its pilot run in 2018, which was aimed at ensuring that beam background levels are safe to install the vertex detector. After the full detector integration, Belle II

has recorded  $55 \text{ fb}^{-1}$  data since 2019. The plan is to collect  $50 \text{ ab}^{-1}$  data by 2029, which is going to make the next decade very interesting for the flavor physics enthusiasts. A short summary on the Belle II experiment is available in Ref. [1].

## III. ANALYSIS TECHNIQUES

The analysis techniques used to study the rare decays can be divided into the following two categories.

- **Exclusive:** A specific  $B$  meson decay mode is reconstructed using its final-state particles e.g., the analysis of the decay  $B^+ \rightarrow K^+ e^+ e^-$  is an exclusive one since it involves the reconstruction and identification of one charged kaon and two electron candidates that are subsequently combined to get the  $B$  meson candidate.
- **Inclusive:** In an inclusive analysis some of the final-state particles are not explicitly reconstructed. The study of  $B \rightarrow X_s \gamma$  is an example of inclusive analysis, where  $X_s$  is defined as any final state having net strangeness of unity. Inclusive decay analyses are further classified into two categories, namely semiinclusive and fully inclusive. Semiinclusive analyses are performed by combining several exclusive decay modes. In comparison, fully inclusive analyses do not rely on specific exclusive decays, rather they involve the reconstruction of the recoiling  $B$  meson with the hadronic or semileptonic tagging procedure. A schematic diagram for these two types of inclusive analysis is shown in Fig. 2. In the hadronic-tag inclusive analysis, the momentum of the signal  $B$  meson can be measured whereas it is not feasible for the semileptonic tag analysis due to the presence of neutrino. Therefore, the former has a lower signal efficiency since it fully reconstructs tag-side  $B$  meson from hadronic decays, which has relatively smaller branching

fraction compared to semileptonic decays. On the other hand, the challenge of a semileptonic tag analysis lies in dealing with the relatively higher background level.

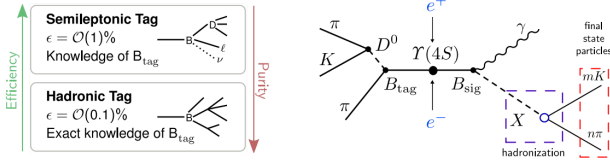


FIG. 2: A hadronic tagged  $B \rightarrow X_s \gamma$  event in the center-of-mass frame.

#### IV. RADIATIVE PENGUIN $B$ DECAYS

In this section, we discuss  $B$  decays that are mediated by  $b \rightarrow s(d)\gamma$  transitions. The leading order Feynman diagram for this process is shown in Fig. 3.

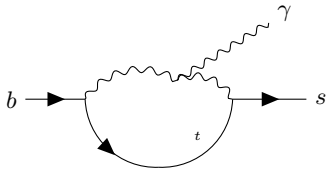


FIG. 3: Leading order Feynman diagram for the  $b \rightarrow s \gamma$  process.

##### A. Rediscovery of the penguin $B$ decay

Among the radiative penguin decays  $B \rightarrow K^* \gamma$  are the first to be rediscovered at Belle II. The isospin asymmetry in these decays ( $\Delta_{0+}$ ) is defined as

$$\Delta_{0+} = \frac{\Gamma(B^0 \rightarrow K^{*0} \gamma) - \Gamma(B^+ \rightarrow K^{*+} \gamma)}{\Gamma(B^0 \rightarrow K^{*0} \gamma) + \Gamma(B^+ \rightarrow K^{*+} \gamma)},$$

which constitutes a clean observable as most of the uncertainties cancel in the ratio. Recent measurement [2] has shown evidence for isospin violation with  $3.1\sigma$  significance, drawing lots of attention to these decays. If this effect is real, then it can be discovered with  $5 \text{ ab}^{-1}$  data at Belle II. The current analysis [3] has been performed with  $2.62 \text{ fb}^{-1}$  data from the following three major decay channels,

- $B^0 \rightarrow K^{*0} [\rightarrow K^+ \pi^-] \gamma$ ,
- $B^+ \rightarrow K^{*+} [\rightarrow K_S^0 \pi^+] \gamma$ , and
- $B^+ \rightarrow K^{*+} [\rightarrow K^+ \pi^0] \gamma$ .

The dominant background is from the light quark production process  $e^+ e^- \rightarrow q \bar{q}$ , also known as continuum background. These events has jetlike structure making them easily distinguishable from spherical  $B \bar{B}$  events. A boosted decision tree classifier, namely FastBDT [4], based on several event-shape variables is trained to suppress continuum background. The selection criterion on the classifier output is optimized by maximizing the figure-of-merit defined as  $S/\sqrt{S+B}$ , where  $S$  and  $B$  are the number of signal and background events in the signal region.

Two kinematic variables called the energy difference ( $\Delta E$ ) and beam-energy constrained mass ( $M_{bc}$ ) are used for the signal  $B$ -meson reconstruction. Here,  $\Delta E$  is the difference between the energy of the reconstructed  $B$  meson and the beam energy in the center-of-mass frame, and  $M_{bc}$  is the mass of the reconstructed  $B$  candidate with its energy being replaced by the beam energy in the center-of-mass frame. A tight requirement  $\Delta E \in [-0.2, 0.08] \text{ GeV}$  is applied to suppress combinatorial background. The signal yield is then obtained by performing an unbinned maximum-likelihood fit to the  $M_{bc}$  distribution. The combined significance of the above three channels exceeds  $5\sigma$ , which is good enough to claim the rediscovery. The obtained results are listed in Table I.

TABLE I: Results of the  $B \rightarrow K^* \gamma$  analysis.

	Signal yield (stat. error only)	Significance
$B^0 \rightarrow K^{*0} [K^+ \pi^-] \gamma$	$19.1 \pm 5.2$	$4.4\sigma$
$B^+ \rightarrow K^{*+} [K^+ \pi^0] \gamma$	$9.8 \pm 3.4$	$3.7\sigma$
$B^+ \rightarrow K^{*+} [K_S^0 \pi^+] \gamma$	$6.6 \pm 3.1$	$2.1\sigma$

##### B. Branching fraction measurement

The branching fraction of inclusive decays are theoretically cleaner over that of exclusive decays, as the form-factor dependence cancel. Profiting from that, the branching fraction of  $\bar{B} \rightarrow X_s \gamma$  provides an important constraint on NP models such as extended Higgs boson sector or supersymmetry [6]. Using an effective theory approach, we can put strong constraints on Wilson coefficients  $C_7$  and  $C_8$  [8]. As described earlier, the inclusive analysis can be performed using the semiinclusive or fully inclusive method. In the first method, the hadronic system  $X_s$  is reconstructed with several exclusive decays that contain an odd number of kaons in the final state. We can separately measure  $\bar{B} \rightarrow X_s \gamma$  and  $\bar{B} \rightarrow X_d \gamma$  only in the semiinclusive method. For the fully inclusive method, where only the hard photon is reconstructed at the signal side, the other  $B$  meson is reconstructed from either hadronic or semileptonic decays.

TABLE II: Sensitivity of  $\text{BF}(\bar{B} \rightarrow X_s \gamma)$  measurement at Belle II in different analysis techniques with  $E_0 = 1.9 \text{ GeV}$ .

Method	Belle II $5 \text{ ab}^{-1}$	Belle II $50 \text{ ab}^{-1}$
Leptonic tag	3.9%	3.2%
Hadronic tag	7.0%	4.2%
Semiinclusive	7.3%	5.7%

So far, all measurements apply a threshold on the photon energy  $E_0 = [1.7, 2.0] \text{ GeV}$ , and some assumption has been made to extrapolate the threshold value to be equal to  $1.6 \text{ GeV}$  to match with the theory prediction. This extrapolation introduces a systematic uncertainty to the result. Another dominant source of uncertainty in the fully inclusive  $\bar{B} \rightarrow X_s \gamma$  analysis arises from neutral hadrons faking the photon. If the  $E_0$  value is taken to be lower, the neutral hadron background increases causing a larger uncertainty. So there is a trade-off between the two types of uncertainty. Dedicated studies on cluster shape at Belle II, which were not tried at Belle, can help improve these systematic uncertainties. In the hadronic tagging method S/B is very good but the signal efficiency is too low. Thanks to the large dataset, the hadronic tagging analysis is possible at Belle II. One of the dominant systematic uncertainties in the semiinclusive method is due to missing decay modes, which can be reduced at Belle II with the help of larger dataset. The relative uncertainties in the measured branching fraction are listed in Table II.

### C. CP violation measurement

The time-integrated CP asymmetry for  $B \rightarrow X_q \gamma$  is defined as

$$\mathcal{A}_{\text{CP}}(\bar{B} \rightarrow X_q \gamma) = \frac{\Gamma(\bar{B} \rightarrow X_q \gamma) - (B \rightarrow X_{\bar{q}} \gamma)}{\Gamma(\bar{B} \rightarrow X_q \gamma) + (B \rightarrow X_{\bar{q}} \gamma)}.$$

Deviation of  $\mathcal{A}_{\text{CP}}(\bar{B} \rightarrow X_{s(d)} \gamma)$  from the SM prediction is a sign of NP that would modify the Wilson coefficients  $C_7$  and  $C_8$  [8]. The theory uncertainties ([9]) in these observables are quite high.

$$\mathcal{A}_{\text{CP}}^{\text{SM}}(\bar{B} \rightarrow X_s \gamma) = [-0.6\%, 2.8\%] \quad (1)$$

$$\mathcal{A}_{\text{CP}}^{\text{SM}}(\bar{B} \rightarrow X_d \gamma) = [-62\%, 14\%] \quad (2)$$

However, a combined measurement CP asymmetry,  $\mathcal{A}_{\text{CP}}^{\text{SM}}(\bar{B} \rightarrow X_{s+d} \gamma) = \mathcal{O}(\Lambda_{\text{QCD}}/m_b)$  is quite low, which is a consequence of the unitarity of the CKM matrix. Belle measurement [10] of  $\mathcal{A}_{\text{CP}}^{\text{SM}}(\bar{B} \rightarrow X_{s+d} \gamma)$ , with the leptonic tag method is consistent with the SM prediction. The total uncertainty being limited by the statistical one is expected to improve with larger Belle II dataset. The dominant systematic uncertainty is

due to the asymmetry of  $B\bar{B}$  backgrounds which are subtracted. The estimation of this asymmetry from sideband will be more accurate with larger dataset. In fact, using the hadronic tag method we can precisely measure the asymmetry of both charged and neutral  $\bar{B} \rightarrow X_s \gamma$  decays and dominant peaking backgrounds. An assumption that the direct CP violation is independent of specific  $X_s$  decay mode while Belle II has the privilege to test this assumption. The systematic uncertainty due to detector asymmetry can also be reduced using large dataset since these are also measured from sideband or control sample.

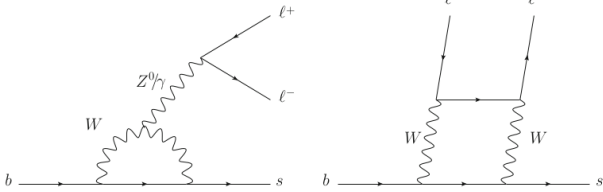
Isospin asymmetry introduced earlier, which has raised interest for  $3.1\sigma$  effect, can also be measured in the inclusive analysis of  $B \rightarrow X_s \gamma$ . Another clean observable is the difference of direct CP asymmetries between the charged and neutral  $B$  decays,  $\Delta A_{\text{CP}} = A_{\text{CP}}(B^+ \rightarrow X_s^+ \gamma) - A_{\text{CP}}(B^0 \rightarrow X_s^0 \gamma)$ , which can be shown as proportional to  $\text{Im}(\frac{C_{8q}}{C_{7\gamma}})$  [9]. In the SM,  $C_7$  and  $C_8$  are both real, therefore  $\Delta A_{\text{CP}}$  is zero, but in several NP models [9, 11, 12]  $\Delta A_{\text{CP}}$  can reach the level of 10%. Since the distinction between charged and neutral  $B$  decays is necessary to measure these two observables, only semiinclusive and hadronic-tag method can be used. So far, measurements [13, 14] are consistent with SM. In these studies statistical uncertainties dominate and can be improved at Belle II. Another dominant uncertainty is due to the production ratio of  $B^+ B^-$  and  $B^0 \bar{B}^0$  from  $\Upsilon(4S)$  decay ( $f_{+-}/f_{00}$ ). At Belle II, this factor can be measured with better precision using double semileptonic decay  $\bar{B} \rightarrow D^* \ell^- \bar{\nu}$ . The sensitivity of these CP violation variables that can be reached at Belle II is listed in Table III.

TABLE III: Sensitivities of CP violation measurement at Belle II in different analysis techniques with  $E_0 = 1.9 \text{ GeV}$ .

Observable	Method	Belle II $5 \text{ ab}^{-1}$	Belle II $50 \text{ ab}^{-1}$
$A_{\text{CP}}(B \rightarrow X_{s+d} \gamma)$	Leptonic tag	1.5%	0.48%
$A_{\text{CP}}(B \rightarrow X_{s+d} \gamma)$	Hadronic tag	2.2%	0.70%
$\Delta A_{\text{CP}}(B \rightarrow X_{s+d} \gamma)$	Semiinclusive	0.98%	0.30%
$\Delta A_{\text{CP}}(B \rightarrow X_{s+d} \gamma)$	Hadronic tag	4.3%	1.3%
$\Delta_{0+}(B \rightarrow X_{s+d} \gamma)$	Semiinclusive	0.81%	0.63%
$\Delta_{0+}(B \rightarrow X_{s+d} \gamma)$	Hadronic tag	2.6%	0.85%

## V. ELECTROWEAK PENGUIN $B$ DECAYS

Electroweak penguin mediated by  $b \rightarrow s \ell^+ \ell^-$  process. The dominant Feynman diagrams in the SM are shown in Fig.4.

FIG. 4: Feynman diagram for  $b \rightarrow s\ell^+\ell^-$  process.

### A. Lepton flavor universality test

Within the SM gauge bosons couple equally to different flavors of lepton. The only non-universality between leptons is their coupling with the Higgs boson as it depends on their mass, but still it has negligible effect on the BF of the decays. Therefore, the ratios of branching fractions, referred to as R-ratios,

$$R_H[q_0^2, q_1^2] = \frac{\int_{q_0^2}^{q_1^2} dq^2 \frac{d\Gamma(B \rightarrow H\mu^+\mu^-)}{dq^2}}{\int_{q_0^2}^{q_1^2} dq^2 \frac{d\Gamma(B \rightarrow He^+e^-)}{dq^2}}$$

are expected to be unity up to corrections from the phase-space difference due to different mass. These R-ratios are very clean observables, as the theoretical uncertainties from CKM factors, form factors and other hadronic effects cancel since they are common in the numerator and denominator. The dilepton invariant mass corresponding to charmonium regions are removed by kinematic selection. This leads two dilepton mass regions, namely low- $q^2$  ( $q^2 \in [1, 6]$   $\text{GeV}^2/c^2$ ) and high- $q^2$  ( $q^2 > 14.4$   $\text{GeV}^2/c^2$ ) regions. Within these two regions theoretical uncertainty is controlled within 10%. For example,  $R_K^{\text{SM}}[1, 6] = 1.000 \pm 0.001$  [17].

From the experimental perspective the main challenge is understanding the difference in performance to reconstruct electrons and muons. The most important difference is introduced by the bremsstrahlung process, which causes electrons to radiate a significant amount of energy. So far, LHCb provided the most precise measurement of both  $R_{K^{(*)}}$  [18, 19] in the low- $q^2$  region. The  $R_{K^{(*)}}$  measurement result is compatible with the SM at the level of 2.5 (2.4) standard deviations.

Previous measurement by Belle [20, 21] has higher uncertainty, and is consistent with both SM and LHCb measurement. Belle already measured R-ratios in the high  $q^2$  bins, which is not possible to measure by LHCb due to experimental constraints. Bremsstrahlung recovery of electron led almost similar efficiency between electron and muon modes. Using larger dataset Belle II measurement can shed light on these ( $R_K, R_{K^*}$ ) anomalies. If the  $R_K$  anomaly is serious and appeared due to NP, we should be able to confirm it with  $5\sigma$  significance using around  $20 \text{ ab}^{-1}$

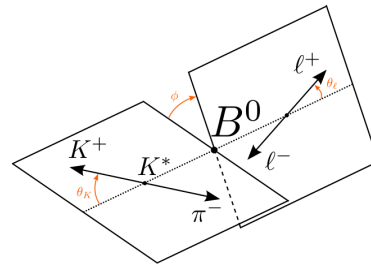
of Belle II data. Thanks to the clean environment, Belle II can also study inclusive  $B \rightarrow X_s \ell^+ \ell^-$  decay and measure  $R_{X_s}$ . Furthermore, Belle II can measure individually charged and neutral channels in  $B \rightarrow K^{*0/+} \ell \ell$ . Overall, Belle II is few steps ahead of other experiments in some perspective. In Table IV sensitivities of R-ratio observables are listed.

TABLE IV: Sensitivities of the observables that would test lepton flavor universality at Belle II.

Observable	Belle II $5 \text{ ab}^{-1}$	Belle II $50 \text{ ab}^{-1}$
$R_K[1,6] \text{ GeV}^2/c^2$	11%	3.6%
$R_K[>14.4] \text{ GeV}^2/c^2$	12%	3.6%
$R_{K^*}[1,6] \text{ GeV}^2/c^2$	10%	3.2%
$R_{K^*}[>14.4] \text{ GeV}^2/c^2$	9.2%	2.8%
$R_{X_s}[1,6] \text{ GeV}^2/c^2$	12%	4.0%
$R_{X_s}[>14.4] \text{ GeV}^2/c^2$	11%	3.4%

### B. Angular analysis of $B \rightarrow K^* \ell^+ \ell^-$

An angular analysis of  $B \rightarrow K^*[K\pi]\ell^+\ell^-$  decays can lead to several observables that are sensitive to NP. The angular distributions are completely described by four independent kinematic variables, chosen as  $q^2 = M_{\ell^+\ell^-}^2$  and three angles  $\cos\theta_\ell$ ,  $\cos\theta_K$ , and  $\phi$ . The angle  $\theta_\ell$  is the angle between the  $\ell^+(\ell^-)$  and the dilepton system in the  $B(\bar{B})$  rest frame. The angle  $\theta_K$  is the angle between the kaon and the  $K^*$  in the  $B(\bar{B})$  rest frame. The angle  $\phi$  is the angle between the decay plane of  $\ell^+\ell^-$  and of  $K^*$ . These angles are described in Fig. 5.

FIG. 5: Definitions of angles in the  $B^0 \rightarrow K^{*0} \ell \ell$  decay

The differential decay rate [22] in terms of angular variables is given by,

$$\frac{d^4\Gamma(\bar{B} \rightarrow \bar{K}^* \ell^+ \ell^-)}{d \cos\theta_\ell d \cos\theta_K d\phi dq^2} = \frac{9}{32\pi} \sum_j I_j f_j(\cos\theta_\ell, \cos\theta_K, \phi),$$

$$\frac{d^4\Gamma(B \rightarrow K^* \ell^+ \ell^-)}{d \cos\theta_\ell d \cos\theta_K d\phi dq^2} = \frac{9}{32\pi} \sum_j \bar{I}_j f_j(\cos\theta_\ell, \cos\theta_K, \phi),$$

where  $I_j$  and  $\bar{I}_j$  are functions of  $q^2$  and depend on the  $K^*$  transitivity amplitude. The angular dependence of each term comes from  $f_j(\cos\theta_\ell, \cos\theta_K, \phi)$ , originating from spherical harmonics associated with different polarisation states of the  $K^*$  and dilepton system. The self-tagging nature of the  $B \rightarrow K^* \ell^+ \ell^-$  decay means that it is possible to determine both CP-averaged and CP-asymmetric quantities that depends on the coefficients,

$$S_i = (I_i + \bar{I}_i) / \frac{d\Gamma}{dq^2}$$

$$A_i = (I_i - \bar{I}_i) / \frac{d\Gamma}{dq^2}$$

It is possible to exploit symmetry relations to construct observables that are free from form-factor uncertainties at leading order in a  $1/m_b$  expansion [23]. It is also possible to build “clean” observables at low  $q^2$  exploiting the form-factor cancellation. This includes so-called  $P'$  series of observables [24] defined as,  $P'_4 = \frac{S_4}{2\sqrt{-S_{2c}S_{2s}}}$ ,  $P'_5 = \frac{S_5}{2\sqrt{-S_{2c}S_{2s}}}$ ,  $P'_6 = \frac{S_7}{2\sqrt{-S_{2c}S_{2s}}}$ ,  $P'_8 = \frac{S_8}{2\sqrt{-S_{2c}S_{2s}}}$ . LHCb measurement[25] found a tension in the  $P'_5$  observable from the  $B^0 \rightarrow K^{*0} \mu^+ \mu^-$  decay. Belle also performed the angular analysis [26], using full dataset with both charged and neutral  $B$  meson. A  $2.6\sigma$  tension is observed in  $P'_5$  of the muon modes in the region  $4 \text{ GeV}^2/c^2 < q^2 < 8 \text{ GeV}^2/c^2$ , which is the same region LHCb claimed as  $P'_5$  anomaly. Lepton flavor dependent measurement of  $P'_5$  can lead to another observable  $Q'_5 = P'_5{}^\mu - P'_5{}^e$ . There are no significant deviation from SM observed in the Belle measurement of  $Q'_5$ .

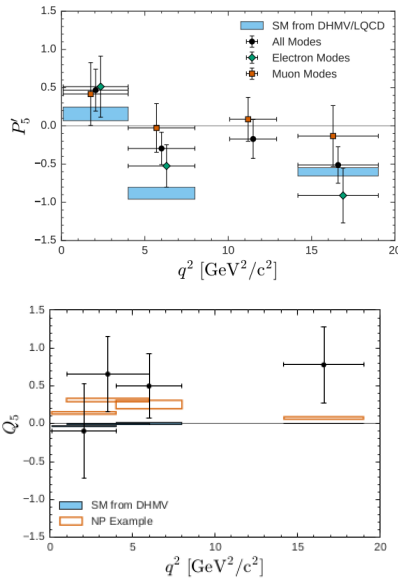


FIG. 6: Measurement of  $P'_5$  and  $Q'_5$  at Belle.

At Belle II, the uncertainty due to peaking background can be reduced by including individual components in the fitted model as these components can be more reliably modeled with larger dataset. The uncertainty in  $P'_5$ , for  $q^2 \in [4, 6] \text{ GeV}^2/c^2$  with  $2.8 \text{ ab}^{-1}$  of Belle II data based on both electron and muon modes will be comparable to the  $3 \text{ fb}^{-1}$  data result of LHCb that uses muon modes only. A naive extrapolation leads to the conclusion that the accuracy that can be achieved on the optimised observables at Belle II with  $50 \text{ ab}^{-1}$  is just 20% lower than the precision that LHCb is expected to reach with  $50 \text{ fb}^{-1}$  of data.

### C. Missing energy channel: $B \rightarrow K^{(*)} \nu \bar{\nu}$

The semileptonic decays mediated by  $b \rightarrow s \nu \bar{\nu}$  is forbidden at tree level involving a single boson exchange. They occur via higher order electroweak penguin (Fig. 7), box diagram (Fig. 8), or tree-level transition involving at least two  $W/Z^0$  bosons (Fig. 9).

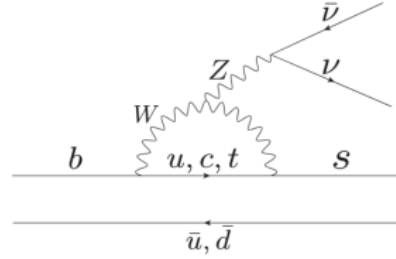


FIG. 7: Electroweak penguin diagram for  $b \rightarrow s \nu \bar{\nu}$ .

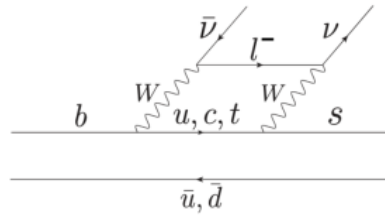


FIG. 8: Box diagram for  $b \rightarrow s \nu \bar{\nu}$ .

An advantage of the  $b \rightarrow s \nu \bar{\nu}$  transition compared to  $b \rightarrow s \ell^+ \ell^-$  is the absence of photon mediated diagrams that lead to a pair of charged leptons. As a consequence, the factorisation of hadronic and leptonic current is exact in case of  $B \rightarrow K^{(*)} \nu \bar{\nu}$ . This makes theoretical predictions more accurate. Measurements of the  $B \rightarrow K^{(*)} \nu \bar{\nu}$  decay rates would in principle allow to extract the  $B \rightarrow K^{(*)}$  form factors to high accuracy.  $B$  decays involving exotic final states e.g., dark matter candidates, are closely

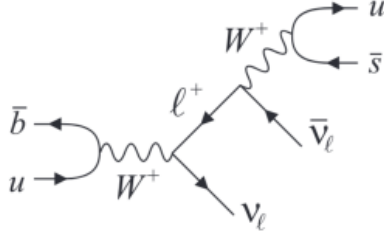


FIG. 9: Tree-level diagram involving two bosons.

TABLE V: Sensitivities of the observables for decays mediated by  $b \rightarrow s\nu\bar{\nu}$ .

Observable	Belle II 5 $\text{ab}^{-1}$	Belle II 50 $\text{ab}^{-1}$
$\text{Br}(B^+ \rightarrow K^+ \nu\bar{\nu})$	30%	11%
$\text{Br}(B^0 \rightarrow K^{*0} \nu\bar{\nu})$	26%	9.6%
$\text{Br}(B^+ \rightarrow K^{*+} \nu\bar{\nu})$	25%	9.3%
$F_L(B^0 \rightarrow K^{*0} \nu\bar{\nu})$	–	0.079
$F_L(B^+ \rightarrow K^{*+} \nu\bar{\nu})$	–	0.077

related to this kind of signals since the missing energy signature on detector are the same. One more observable which is sensitive to NP is the  $K^*$  longitudinal polarisation fraction ( $F_L$ ) in  $B \rightarrow K^* \nu\bar{\nu}$ . The polarization fraction can be extracted from the angu-

lar distribution in the invariant mass of the neutrino-antineutrino pair and the angle between the  $K^*$  flight direction in the  $B$  rest frame and the  $K$  flight direction in the  $K\pi$  rest frame. Ref. [16] predicts  $F_L^{\text{SM}} = 0.47 \pm 0.03$ . Another study [15] shows the presence of NP operator in operator product expansion,  $\mathcal{O}_R = \frac{e^2}{16\pi^2} (\bar{s}\gamma_\mu P_R b)(\bar{\nu}\gamma_\mu(1-\gamma_5)\nu)$  is reflected in the observable  $F_L$ . In other words, this observable is sensitive to right-handed quark current.

In the SM, the branching fractions of  $B \rightarrow K^+ \nu\bar{\nu}$  and  $K^* \nu\bar{\nu}$  are  $(4.6 \pm 0.5) \times 10^{-6}$  and  $(9.6 \pm 0.9) \times 10^{-6}$ , respectively. None of the decays has been yet discovered experimentally. They are expected to be observed with first  $10 \text{ab}^{-1}$  of data. To measure  $F_L$  larger data sample is required. Based on a toy Monte Carlo study, it is estimated that with  $50 \text{ab}^{-1}$  the uncertainty of  $F_L$  will be 0.11. The sensitivities of the observables are listed in Table V.

## VI. SUMMARY

The clean environment at Belle II grants access to several unique observables in rare  $B$  decays. Starting with the rediscovery of  $B \rightarrow K^* \gamma$ , Belle II is on its way to rediscover other suppressed penguin decays. We expect to provide strong model-independent constraints on new physics, thanks to the large data sample of Belle II.

- 
- [1] J. Bennett, J. Phys.: Conf. Ser. **770** 012044 (2016).
  - [2] T. Horiguchi et al. (Belle Collaboration), Phys. Rev. Lett. **119**, 191802 (2017).
  - [3] <https://docs.belle2.org/record/1593/files/BELLE2-NOTE-PL-2019-021.pdf>
  - [4] T. Keck, arXiv:1609.06119 (2016).
  - [5] M. Misiak et al., Phys. Rev. Lett. **114**, 221801 (2015).
  - [6] O. Deschamps et al., Phys. Rev. D **82**, 073012 (2010).
  - [7] A. Abdesselam et al. (Belle Collaboration), arxiv:1608.02344 (2016).
  - [8] P. Gambino and M. Misiak, Nucl. Phys. B **611**, 338 (2001).
  - [9] M. Benzke et al., Phys. Rev. Lett. **106**, 141801 (2011).
  - [10] L. Pesantez et al. (Belle Collaboration), Phys. Rev. Lett. **114**, 151601 (2015).
  - [11] R. Malm, M. Neubert and C. Schmell, J. High Energy Phys. **04**, 042 (2016).
  - [12] M. Endo et al., J. High Energy Phys. **04**, 019 (2018).
  - [13] B. Aubert et al. (BaBar Collaboration), Phys. Rev. D **72**, 052004 (2005).
  - [14] S. Watanuki et al. (Belle Collaboration), Phys. Rev. D **99**, 3 (2019).
  - [15] W. Altmannshofer et al., J. High Energy Phys. **04**, 022 (2009).
  - [16] A. J. Buras et al., J. High Energy Phys. **02**, 184 (2015).
  - [17] C. Bobeth, G. Hiller and G. Piranishvili, J. High Energy Phys. **12**, 040 (2007).
  - [18] R. Aaij et al. (LHCb Collaboration), Phys. Rev. Lett. **122**, 191801 (2019).
  - [19] R. Aaij et al. (LHCb Collaboration), J. High Energy Phys. **08**, 055 (2017).
  - [20] S. Choudhury et al. (Belle Collaboration), arXiv:1908.01848 (2019). rkbabar J. P. Lees et al. (BaBar Collaboration), Phys. Rev. D **86**, 032012 (2012).
  - [21] J. T. Wei et al. (Belle Collaboration), Phys. Rev. Lett. **103**, 171801 (2009).
  - [22] W. Altmannshofer et al., J. High Energy Phys. **01**, 019 (2009).
  - [23] F. Kruger and J. Matias, Phys. Rev. D **71**, 094009 (2005).
  - [24] S. Descotes-Genon et al., J. High Energy Phys. **05**, 137 (2013).
  - [25] R. Aaij et al. (LHCb Collaboration), J. High Energy Phys. **02**, 104 (2016).
  - [26] W. Altmannshofer et al., Eur. Phys. J. C **77**, 377 (2017).